934 *Biochemistry* **2010,** *49,* 934–944
DOI: 10.1021/bi901985b

BIOCHEMISTRY
including biophysical chemistry & molecular biology
Article

Crystal Structure of the Cofactor-Independent Monooxygenase SnoaB from *Streptomyces nogalater*: Implications for the Reaction Mechanism[†]

Thadee Grocholski,[‡,||] Hanna Koskiniemi,[§,||] Ylva Lindqvist,[§] Pekka Mäntsälä,[‡] Jarmo Niemi,*[,‡] and Gunter Schneider*[,§]

[‡]*Department of Biochemistry and Food Chemistry, University of Turku, FIN-20014 Turku, Finland and* [§]*Department of Medical Biochemistry and Biophysics, Karolinska Institutet, S-171 77 Stockholm, Sweden* [||]*Joint first authors*

Received November 18, 2009; Revised Manuscript Received January 5, 2010

ABSTRACT: SnoaB is a cofactor-independent monooxygenase that catalyzes the conversion of 12-deoxynogalonic acid to nogalonic acid in the biosynthesis of the aromatic polyketide nogalamycin in *Streptomyces nogalater*. *In vitro* $^{18}O_2$ experiments establish that the oxygen atom incorporated into the substrate is derived from molecular oxygen. The crystal structure of the enzyme was determined in two different space groups to 1.7 and 1.9 Å resolution, respectively. The enzyme displays the ferredoxin fold, with the characteristic β-strand exchange at the dimer interface. The crystal structures reveal a putative catalytic triad involving two asparagine residues, Asn18 and Asn63, and a water molecule, which may play important roles in the enzymatic reaction. Site-directed mutagenesis experiments, replacing the two asparagines individually by alanine, led to a 100-fold drop in enzymatic activity. Replacement of an invariant tryptophan residue in the active site of the enzyme by phenylalanine also resulted in an enzyme variant with about 1% residual activity. Taken together, our findings are most consistent with a carbanion mechanism where the deprotonated substrate reacts with molecular oxygen via one electron transfer and formation of a caged radical.

Because direct addition of O_2 to organic molecules is a spin-forbidden reaction, most mono- and dioxygenases utilize either transition metals or organic cofactors to overcome the spin -barrier (*1*, *2*). Recent structural and functional studies have however established a class of mono- and dioxygenases without the need for cofactors or metal ions (*2*, *3*). These cofactor-independent oxygenases comprise diverse enzyme families, not related in amino acid sequence or protein fold (*4*−*10*).

One of these enzyme families is found in the biosynthetic pathways of aromatic polyketides in streptomycetes. SnoaB, a member of this sequence family, participates in the biosynthesis of the anthracycline nogalamycin in *Streptomyces nogalater* (*11*). The *snoaB* gene codes for a small enzyme of 118 amino acids (molecular mass 13.1 kDa) (*12*) that catalyzes the oxygenation of the C-12 carbon atom of the substrate 12-deoxynogalonic acid (Figure 1). The reaction yields a quinone product, nogalonic acid, which is the first isolable intermediate in the biosynthesis of the aromatic polyketide nogalamycin (*11*). The formation of the quinone is a common modification of the aglycone core and occurs in many aromatic polyketides. Thus it is not surprising that SnoaB has homologues in biosynthetic pathways of other polyketides, such as AknX in the biosynthesis of aclacinomycin (*13*), TcmH in tetracenomycin biosynthesis (*14*), DnrG/DauG in daunomycin biosynthesis (*15*), and ActVA-Orf6 in the actinorhodin biosynthesis route (*16*). In actinorhodin biosynthesis in *Streptomyces coelicolor*, the oxygenation step is preferentially catalyzed by an alternative enzymatic system, the flavin-dependent two-component oxygenase ActVA-Orf5/ActVB (*17*). ActVA-Orf6 appears to catalyze this step only if the function of ActVA-Orf5/ActVB is compromised. The gene cluster for nogalamycin biosynthesis in *S. nogalater* does not contain, however, any sequences homologous to this two-component oxygenase system, suggesting that in nogalamycin biosynthesis this tailoring step is catalyzed only by SnoaB.

Biochemical characterization of AknX (*18*), TcmH (*19*), and ActVA-Orf6 (*16*) has shown that these enzymes do not contain bound metal ions or prosthetic groups typical for oxygenases. Earlier $^{18}O_2$ feeding studies suggested, on the other hand, that one of the aromatic polyketide quinone oxygens is derived from molecular oxygen while the other oxygen originates from the precursor acid (*20*, *21*). However, to our knowledge, it has not yet been demonstrated *in vitro* that oxygenases from the SnoaB family indeed utilize molecular oxygen in the reaction. Two different reaction mechanisms have been suggested for the SnoaB-like monooxygenases of polyketide biosynthesis, both relying on substrate assistance in the activation of oxygen. For AknX and ActVA-Orf6, it was proposed that the reaction proceeds via a carbanion intermediate (*4*, *18*). Alternatively, the oxygen may be activated by a substrate/enzyme radical intermediate (*19*).

We have recombinantly produced SnoaB in *Escherichia coli* and determined its three-dimensional structure to 1.7 Å in two different crystal forms. The enzyme is a homodimer and resembles ActVA-Orf6 despite the absence of significant overall sequence identity (16%). Based on the structure putative catalytic residues were examined by site-directed mutagenesis. Structural and biochemical data are consistent with an enzymatic mechanism that assumes formation of a carbanion intermediate during catalysis. A comparison with ActVA-Orf6 suggests, however, considerable differences in the structural basis for substrate/oxygen activation within this enzyme family.

[†]This work was supported by the Swedish Science Council and the Finnish Academy (Grant 121688).

*To whom correspondence should be addressed. J.N.: e-mail, jarnie@utu.fi; phone, +358 2 3336877; fax, +358 2 3336860. G.S.: e-mail, gunter.schneider@ki.se; phone, +46 8 52487675; fax, +46 8 327626.

 Published on Web 01/06/2010

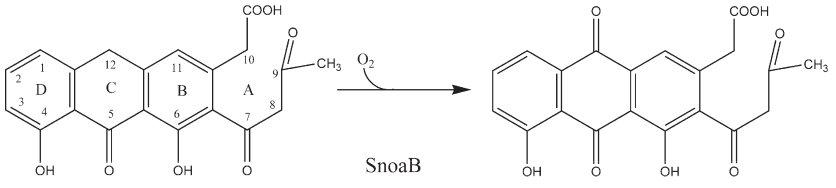

FIGURE 1: The reaction catalyzed by SnoaB. Numbering of the carbon atoms and labeling of the tetracyclic ring system of the anthracyclines are also shown. Ring A will be closed in the biosynthetic step following SnoaB, after methylation by SnoaC, by the action of the polyketide cyclase SnoaL (*51*).

MATERIALS AND METHODS

Expression Constructs for SnoaB. Design of a plasmid carrying the gene coding for SnoaB, including an N-terminal polyhistidine tag (SnoaB-N), has been described previously (*12*). For a construct with a His tag at the C-terminus (SnoaB-C), *snoaB* was amplified by PCR from the plasmid template pSn15 (*11*) using Phusion DNA polymerase (Finnzymes). The PCR product was digested and ligated into a pBAD/HisB vector (Invitrogen). The construct codes for a protein with an additional amino acid at the N-terminus (MAPTR... instead of MPTR...) and a polyhistidine tag (...RHHHHHH-) at the C-terminus. The resulting plasmid was transformed into the *E. coli* strain TOP10 (Invitrogen), and the construct was verified by DNA sequencing.

Mutagenesis. The single SnoaB mutations Asn18Ala, His49Ala, Asn63Ala, Trp67Phe, and Arg90Gln were introduced into the expression vector for SnoaB-N by the four-primer method (*22*). Amplified PCR products were digested and ligated into a modified pBAD/HisB vector (Invitrogen). All constructs were verified by DNA sequencing.

Expression and Purification. SnoaB-N, SnoaB-N mutants, and SnoaB-C constructs were expressed and the enzymes purified using a protocol previously described (*12*). Yields of the SnoaB-N mutants and SnoaB-C were ranging from 5 to 40 mg/L of culture medium. Sample homogeneity was analyzed by SDS−PAGE. Purified enzymes were stored in 50 mM Tris-HCl, pH 8.0, containing 75 mM NaCl and 50% (v/v) glycerol at −20 or −80 °C until further use. Enzyme concentrations were determined at 280 nm using absorption coefficients obtained by ProtParam (*23*).

Anthraquinone Substrate Analogues. Anthraquinones were purchased from Sigma and TCI Europe. Reduction of anthraquinones to their corresponding anthrone analogues and purification were performed as previously described (*24*). Nogalonic acid was produced with a construct similar to pSY21c (*25*).

Assay and Kinetic Analysis of SnoaB Oxygenase Activity. The reaction mixture consisted of 200 μL (final volume) of 64% (v/v) 0.1 M TES, pH 7.0, and 36% (v/v) 2-methoxyethanol. Stock solutions of anthrone analogues were made to 8 mM in 2-methoxyethanol and added to the reaction mixture to final concentrations of 12−250 μM. For each anthrone analogue, concentrations of SnoaB-N, SnoaB-C, and mutant SnoaBs were optimized such that reactions could be followed in 2−5 min at 22 °C. Within this time scale, nonenzymatic oxidation of the anthrone analogues was not observed. The oxygenase activity of SnoaB was followed spectrophotometrically at the wavelength characteristic for each anthraquinone analogue. The reaction was started by the addition of the enzyme to the reaction mixture. Nonlinear regression analysis of the initial reaction rates was performed using Origin Pro (version 7.0). Standard curves of the anthraquinone analogues were used to quantify the reaction rates.

Oxygen Incorporation Assay. Oxygen incorporation into the product of SnoaB, isolation of the product, and mass determination by mass spectrometry were performed using protocols described previously (*26*, *27*). Enzymatic reactions were carried out in a Thunberg cuvette in the presence of $^{16}O_2$ or $^{18}O_2$, respectively. An equimolar amount of SnoaB and dithranol was used to ensure the reaction went to completion in less than 1 min. The substrate dithranol, from a control experiment without addition of SnoaB, and the reaction products obtained with $^{16}O_2$ and $^{18}O_2$ in the presence of SnoaB were extracted with chloroform. Their mass was determined by mass spectrometry as described previously (*26*). The reaction products obtained in the presence of SnoaB were identical in UV/visible absorption spectra and HPLC profiles to the corresponding commercially available anthraquinones.

Crystallization and Data Collection. The storage buffer of SnoaB-C was exchanged to 25 mM Hepes, pH 7.5, 50 mM NaCl, and 5% (v/v) glycerol with the PD-10 desalting columns (GE Healthcare). The protein was incubated with a product analogue, danthrone (saturated in acetonitrile), for 1 h on ice with the ligand approximately 5 times in molar excess over the protein. The protein was subsequently concentrated to approximately 15 mg/mL as estimated with Bradford's assay using the Microsep and Nanosep 3K Omega centrifugal concentrator devices (PALL Corp.) at +4 °C. Before the crystallization experiments, the protein was filtered with Ultrafree MC 0.1 μm filters (Millipore). Crystals of SnoaB-C were obtained with the Nextal JCSG+ random matrix screen (Qiagen). They grew in a drop with a total volume of 0.3 μL with 0.1 μL of protein solution and 0.2 μL of reservoir solution consisting of 2.0 M ammonium sulfate, 100 mM sodium cacodylate buffer, pH 6.5, and 0.2 M NaCl. Crystals appeared after 2 months at +4 °C. Prior to flash-freezing in liquid nitrogen the crystals were soaked quickly in a solution containing 75% (v/v) reservoir solution and 25% (v/v) ethylene glycol. A data set to 1.9 Å resolution was collected at beamline ID23-1, ESRF, Grenoble, France, at 100 K. Based on the analysis of the diffraction pattern, scaling statistics, and, later on, the molecular replacement solution, the crystal was assigned to the space group $P4_12_12$ with unit cell dimensions $a = b = 82.7$ Å and $c = 83.4$ Å. The asymmetric unit contains two enzyme subunits, giving a solvent content of 52%.

The constructs with an N-terminal polyhistidine tag (SnoaB-N), both wild-type and mutant enzymes, were crystallized as previously described (*12*), but danthrone was omitted from the crystallization solution. Crystals of the wild-type protein were soaked with the natural product, nogalonic acid,

Table 1: Data Collection and Refinement Statistics

	SnoaB-C	SnoaB-N	SnoaB-N Asn63Ala
space group	$P4_12_12$	$P2_12_12$	$P2_12_12$
cell axis *a* (Å)	82.7	58.3	57.8
cell axis *b* (Å)	82.7	112.4	111.6
cell axis *c* (Å)	83.4	47.1	48.1
resolution (Å)	58.70−1.90 (2.00−1.90)	50.00−1.70 (1.79−1.70)	30.00−2.50 (2.64−2.50)
R_{sym} (%)	9.5 (44.1)	3.5 (35.4)	10.3 (57.1)
$I/\sigma(I)$	19.6 (6.5)	24.8 (2.6)	13.2 (2.0)
completeness (%)	100.0 (100.0)	94.8 (73.1)	99.8 (99.3)
multiplicity	14.8 (15.2)	5.1 (2.8)	6.0 (3.7)
no. of reflections	347364 (50869)	169337 (9986)	67492 (5873)
no. of unique reflections	23455 (3344)	32939 (3585)	11301 (1591)
Wilson *B*-factor (Å^2)	22.1	23.9	52.5
beamline	ID23-1	ID14-2	ID14-2
R_{work} (%)	18.6	17.0	21.0
R_{free} (%)	22.7	20.9	26.2
rmsd from ideal geometry			
bond length (Å)	0.007	0.015	0.012
bond angle (deg)	1.00	1.37	1.30
no. of atoms			
protein	1643	2377	2364
ligands/ions	34	15	2
water molecules	163	196	34
B-factor (Å^2)[a]			
protein	26.2	19.0	33.3
ligands	36.7	41.0	44.5
solvent	39.8	29.7	31.2
Ramachandran plot (%)			
most favored	96.5	98.1	95.0
additionally allowed	3.5	1.9	5.0
generously allowed	0	0	0
disallowed	0	0	0

[a] *B*-factors excluding the TLS contributions.

Table 2: Substrate Analogues Tested with SnoaB

compound	product formed	wavelength (nm) measured for formed product	specific activity (μM min^{-1} mg^{-1})	relative V_{max} (%)
dithranol	dantron	430	6.3 ± 1.1	100
1-hydroxyanthrone	1-hydroxyanthraquinone	405	0.07 ± 0.01	1.2
anthrone	anthraquinone	331	0.017 ±0.003	0.3
1,4-dihydroxyathrone	quinizarin	472	no reaction	0.0

Table 3: Kinetic Parameters of Wild-Type and Mutant SnoaB

SnoaB variants	V_{max} (μmol min^{-1} mg^{-1})	relative V_{max} (%)	k_{cat} (s^{-1})	K_M (μM)	k_{cat}/K_M (M^{-1} s^{-1})
SnoaB-C	6.1 ± 0.5	96.5	1.4	94 ± 19	1.5×10^4
SnoaB-N	6.3 ± 1.1	100	1.5	140 ± 33	1.1×10^4
Asn18Ala	0.1 ± 0.01	1.6	0.03	120 ± 17	2.2×10^2
His49Ala	1.3 ± 0.002	20.6	0.3	150 ± 21	2.0×10^3
Asn63Ala	0.07 ± 0.004	1.1	0.02	68 ± 11	2.3×10^2
Trp67Phe	0.06 ± 0.008	1.0	0.02	220 ± 45	68
Arg90Gln	1.2 ± 0.060	19.0	0.3	113 ± 12	2.5×10^3

for 10 days at +4 °C in a solution containing 20% (v/v) ligand saturated in methanol, 10% (v/v) ethylene glycol, and 70% (v/v) reservoir solution. A crystal was flash-frozen in liquid nitrogen, and data were collected at beamline ID14-2 at the ESRF, Grenoble, France. The crystal belonged to the space group $P2_12_12$ with unit cell dimensions a = 58.3 Å, b = 112.4 Å, and c = 47.1 Å. Three molecules in the asymmetric unit correspond to a solvent content of 32% with a V_M of 1.8 Å^3 Da^{-1}.

A data set to a resolution of 2.5 Å was collected from a crystal of the mutant Asn63Ala. The crystal had been soaked with a substrate analogue, chrysarobin, at +4 °C for 4 days in a solution containing 10% (v/v) ligand saturated in methanol, 80% (v/v) reservoir solution, and 10% (v/v) DMSO to improve the solubility of the ligand. The crystals of the Asn63Ala mutant belonged to the same orthorhombic space group as the wild type with similar cell dimensions (Table 1). Crystals of the mutants Asn18Ala and Trp67Phe typically diffracted only to low resolution

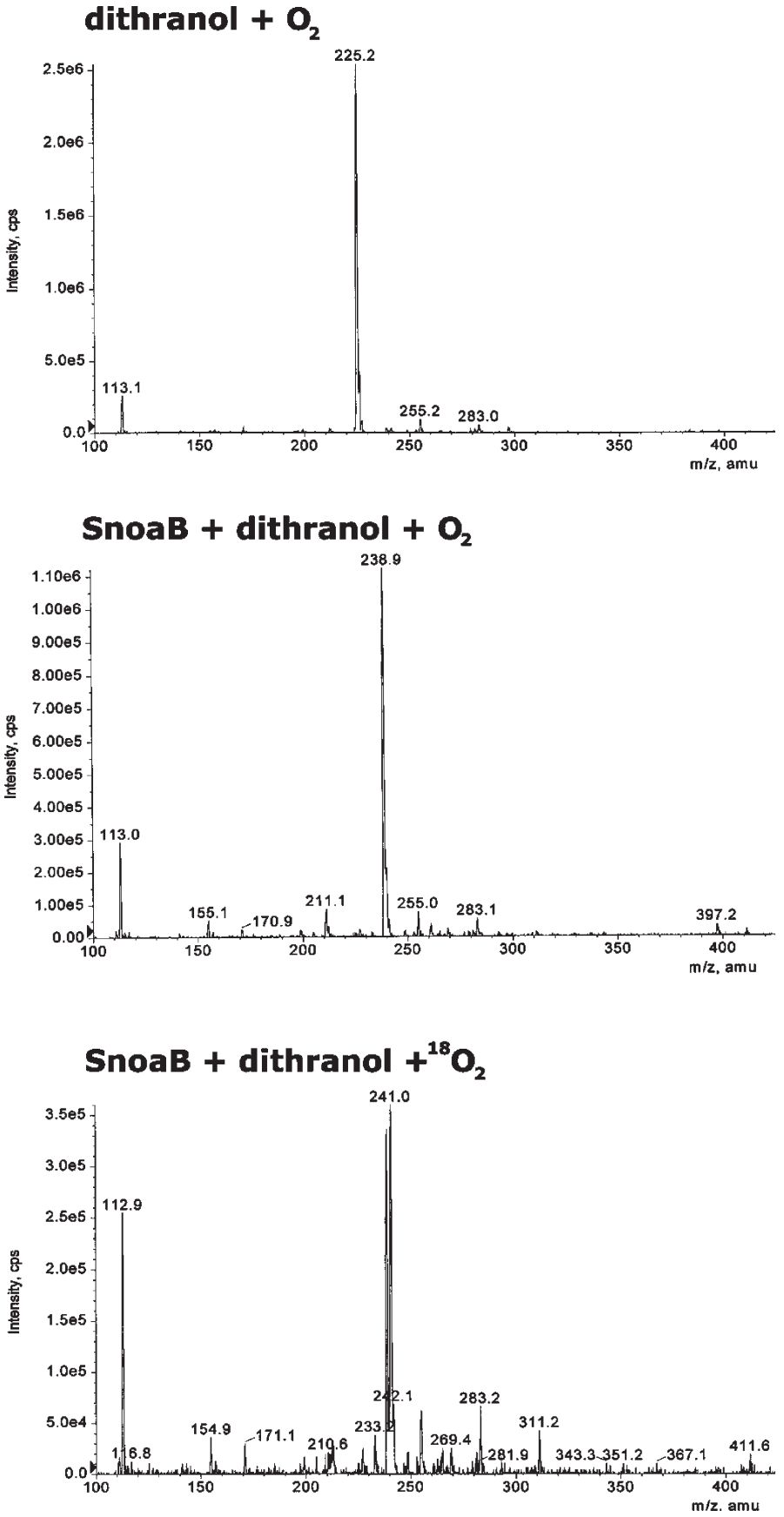

FIGURE 2: ESI-mass spectrometry results from the *in vitro* reaction of dithranol with $^{16}O_2$ or $^{18}O_2$, catalyzed by SnoaB. The 2 Da mass differences in the products of the reaction with $^{16}O_2$ or $^{18}O_2$, respectively, demonstrates the incorporation of oxygen derived from molecular oxygen during the monooxygenase reaction.

and suffered from severe anisotropy, and thus no diffraction data were collected. All diffraction data were processed with Mosflm (*28*) and scaled with Scala from the CCP4 suite (*29*). The data collection statistics of the data sets are given in Table 1.

Structure Determination and Refinement. The structure of SnoaB-C was determined by molecular replacement using a polyserine model of the dimer of ActVA-Orf6 (PDB code 1lq9; amino acid sequence identity to SnoaB, 16%) as search model and the program Phaser (*30*). Five percent of the reflections were omitted from refinement for cross-validation. The obtained electron density map, after a few cycles of rigid body refinement, allowed unambiguous assignment of the amino acid sequence. The structure was further refined with alternating cycles with the program Refmac5.5 (*31*) and manual inspection in COOT (*32*). NCS restraints were applied where appropriate. Water molecules were assigned based on peak heights of residual electron density, *B*-factors, and hydrogen-bonding patterns. Toward the end of the procedure, TLS refinement (*33*) was applied. Optimal TLS groups were defined with the server TLSMD (*34*). Finally, composite omit maps were generated with CNSsolve 1.2 (*35*).

Subsequently, the structure of SnoaB-N was determined by molecular replacement with Phaser (*30*), using the SnoaB-C structure as a search model. Refinement of SnoaB-N and the Asn63Ala mutant followed the procedure as outlined above. The final R/R_{free} for SnoaB-C are 18.6%/22.7%, for SnoaB-N 17.0%/20.9%, and for the mutant Asn63Ala 21.0%/26.2%. The refined crystallographic model of SnoaB-N consists of three protein subunits comprising residues 11−107 (chain A), 11−108 (chain B), and 10−106 (chain C), three molecules of ethylene glycol, three chloride ions, and 196 water molecules. The final model for SnoaB-C contains two enzyme subunits, comprising residues 11−108 (chain A) and 12−108 (chain B), 163 water molecules, four sulfate ions, two chloride ions, and three ethylene glycol molecules. Details of the crystallographic data and refinement statistics are given in Table 1. The crystallographic data for SnoaB-N, SnoaB-C, and Asn63Ala have been deposited with the Protein Data Bank with accession codes 3kng (SnoaB-C), 3kg0 (SnoaB-N), and 3kg1 (Asn63Ala mutant), respectively.

The quality of the structures was analyzed by Procheck (*36*) and MolProbity (*37*). The surface area of the dimer interface was calculated with the PISA server (*38*). The PRODRG server (*39*) and Sketcher from the CCP4 suite were used to prepare models of substrates and ligands. Sequence alignments were made with ClustalW (*40*) and structural alignments with PromalS3D (*41*). Figures were prepared with PyMol (*42*).

RESULTS

SnoaB Is a Stable Oxygenase That Utilizes Molecular Oxygen. The two expression constructs produce stable, active enzymes that can be purified to electrophoretic homogeneity in a straightforward manner. Since the most reproducible crystals were grown using SnoaB-N, this enzyme variant was used for all biochemical work. SnoaB-N is very stable toward heat and organic solvents. It retains enzymatic activity after heating to 95 °C for 5 min and in 95% (v/v) acetonitrile. A similar thermostability has been described for the SnoaB homologue AknX (*18*).

Since the natural substrate was not available, we tested a range of anthrones as potential substrates (Table 2). Most of these compounds were rather poor substrates, with only dithranol showing significant activity. With dithranol as substrate SnoaB-N had a maximal velocity V_{max} of 6.3 μM^{-1} min^{-1} (mg of protein)$^{-1}$, which corresponds to a k_{cat} value of 1.5 s^{-1} and a K_M value of 140 μM (Table 3). SnoaB-catalyzed oxidation of dithranol also occurred in the absence of light.

Table 4: Effect of Metal Ions and EDTA on the Catalytic Activity of SnoaB

additive	concn (μM)	activity (%)
–	–	100
EDTA	100	97.8
EDTA	1000	92.0
$FeSO_4$	100	69.2
$Fe_2(SO_4)_3$	100	103.4
$MgSO_4$	100	92.9
$ZnSO_4$	100	108.8
$CaCl_2$	100	91.0
$MnSO_4$	100	104.3
$CoSO_4$	100	90.3
$CuSO_4$	100	0.5

In order to reveal the origin of the incorporated oxygen atom in the SnoaB-catalyzed reaction, the enzyme was allowed to react with dithranol under $^{18}O_2$ atmosphere, and the product was analyzed by mass spectrometry. The analysis showed that the product has a molecular mass of 241 Da, 2 Da more than the molecule produced under normal atmosphere (Figure 2). These data establish that SnoaB uses molecular oxygen as the oxygen source also *in vitro*.

Addition of metal salts to the reaction mixture did not result in a significant increase in catalytic activity. While most metal ions caused only minor variations of catalytic activity, Fe(II) and Cu(II) ions inhibited the enzyme to various degrees (Table 4). EDTA at final concentrations of 1 mM did not significantly inhibit the enzyme. These findings do not support a metal dependence of SnoaB, consistent with the crystallographic analysis that did not reveal any metal ions bound to the enzyme.

Structure Determination. The crystal structure of SnoaB was determined in two different crystal forms and refined to high resolution. The asymmetric unit of the tetragonal crystal form contains the biological dimer, whereas in the orthorhombic crystals the dimers are generated by crystallographic symmetry. As expected from the resolution of the data, the electron density is of very good quality in both space groups. The polyhistidine tags and N- and C-termini are not visible, indicating high flexibility/disorder of these parts of the polypeptide chain. The structures of the enzyme subunits in the two crystal forms are very similar: superposition of subunits from the tetragonal and orthorhombic crystals yields rmsd values for equivalent Cα atoms in the range of 0.4 and 0.8 Å. The structural differences between the subunits are localized mainly in the loop comprising residues 53−56 and the N- and C-terminal regions of the polypeptide chain. Four sulfate ions from the crystallization mixture are well ordered in the tetragonal crystal form, and three of these participate in crystal packing between adjacent protein molecules.

Overall Structure. The overall structure of the subunit is a ferredoxin-like α + β sandwich (Figure 3A). The core of the molecule is a five-stranded antiparallel β-sheet, in which one of the strands (S5) is provided from the second subunit via β-strand exchange (Figure 3B). The β-sheet is flanked on one side by three α-helices, and the active site is formed between the helices and the β-sheet. All of the secondary structure elements of this small enzyme are involved in forming the active site cavity.

SnoaB forms a dimer in the crystal, consistent with cross-linking studies that had suggested a dimeric structure also in solution (*12*). The mode of oligomerization is likely to be the same, as it is highly conserved not only between different crystal forms of SnoaB but also between structural homologues. The

overall dimensions of the monomer are approximately 15 × 35 × 37 Å and those of the dimer about 25 × 35 × 50 Å. The dimer interface accounts for a significant part (20%) of the protein surface: the buried area in the dimer interface is approximately 1300 Å^2, with a the total solvent-accessible area of 6500 Å^2. In both space groups the dimer is formed via the β-sheets, and the two subunits are related by a 2-fold symmetry axis. The two β-sheets form an imperfect β-barrel (Figure 3B). A total of 37 of the 98 ordered residues of the subunit participate in the dimer interactions. The dimer is maintained by extensive hydrophobic interactions and more than 20 hydrogen bonds. In addition, there are two salt bridges between residues Arg103 (subunit A) and Glu30 (subunit B) and vice versa. The β-strand exchange contributes significantly to the formation and stabilization of the dimer, which is often visible as an additional band on SDS−PAGE.

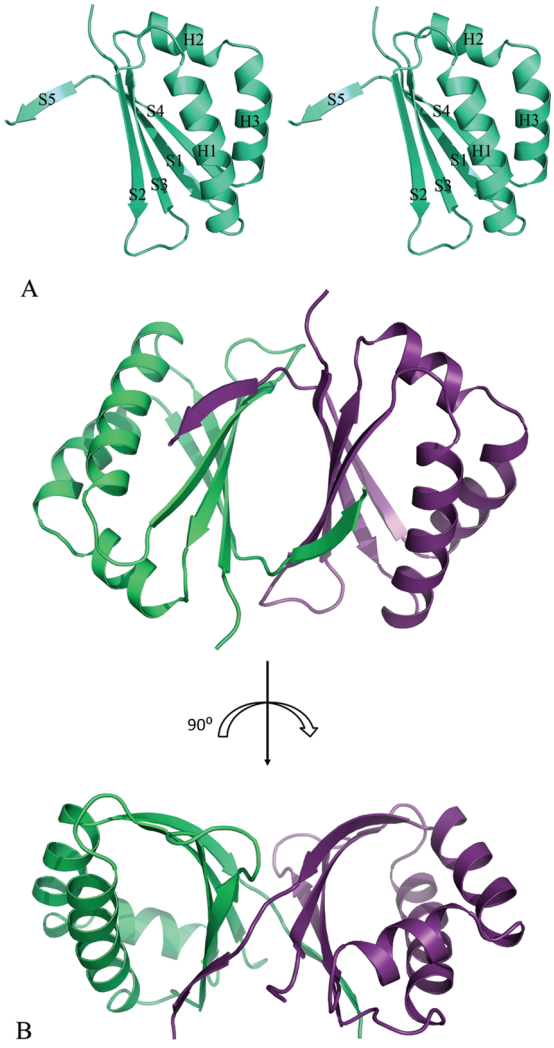

FIGURE 3: (A) Stereoview of the subunit of SnoaB with the secondary structure elements labeled. (B) Quaternary structure of SnoaB. The two subunits are colored in green and purple, respectively.

Sequence Comparisons. A BLAST search against all redundant protein sequences in GenBank reveals a number of homologous oxygenases or putative oxygenases of *Streptomyces* and other bacterial origin. The closest sequence homologues are AknX from *Streptomyces* sp. SPB74 (GenBank accession code EDY42533.1) with an amino acid sequence identity of 49%, a monooxygenase from *Streptomyces steffisburgensis* (id CAJ42321.1) with 45% identity, an oxygenase from *Streptomyces peucetius* (id AAA65205.1) with 45% identity, and CosX from *Streptomyces olindensis* (id ABC00737.1) with 43% identity. The catalytic residues Asn18, Asn63, and Trp67 are conserved in these enzymes (Figure 4). The conservation of the PGF motif has been noted previously (*2*, *18*). The structure of SnoaB suggests that the first two residues of this motif are likely to be important in stabilization of the turn between helix H1 and β-strand S2, whereas the phenylalanine side chain contributes to the topology of the active site.

Comparison to Related Structures. A DaliLite (*43*) search against all structures in the Protein Data Bank reveals a number of structural homologues of various origins, reflecting the ubiquitousness of the ferredoxin fold. However, even the closest structural relatives with Z scores around 10 show only weak amino acid sequence identity to SnoaB; the highest, 17%, is the hypothetical protein TT1380 from *Thermus thermophilus* (PDB accession code 1IUJ) (*44*). Most of the homologues are of unknown function or described as putative oxygenases, and only a few are characterized biochemically, for instance, the iron-dependent sulfur oxygenase reductase from the thermoacidophilic

```
                1        10        20        30        40        50      57
SnoaB      ------MPTRVNDGVDADEVTFVNRFTVHG---APAEFESVFA-R-TAAFFARQPGFVRHTLLRER-DK-------
ActVA-Orf6 ---------MAEVNDPRVGFVAVVTFPVDGP-ATQHKLVELATGGVQ-EWIREVPGFLSATYHAST—D--------
YgiN       ------------------MLTVIAEIRTRPGQHHRQAVLDQFA-K-IVPTVLKEEGCHGYAPMVDCAAGVSFQSMA
AknX       ------MTDRESDAGEDGAVTFLNTFTVHA---EAGVFEEEFA-R-TSAFMARQPGFVRHTLCRHT-EQ-------
TcmH       ------MAT---ISPSPDLFTLVNVFGVAP---EKQRELRDHLVQVTEDLIRHMPGFVSATFHLSR-DG-------
peucetius  ------MPQPEPNDAGSGSVTFVNRFTLSG---SAEDFEAAFA-E-TAEFLCRRPGFRWHALLVPA-DTGPGSADA
steffi     ------MPTHKYDATDSGIVTFVNQFTVHS---SPEEFEKIFA-E-VSEFMAEQPGFIQYTLSRSI-DEDK-----
CosX       MRSTDPMSADQPGPASGGPATFVNSFTLRT---TPEEFEDVFA-R-TARFMERQPGFLGYTLVRHL-EQ-------

             60        70        80        90              100       110     118
SnoaB      DNSYVNIAVWTDHDAFRR-ALAQPGFLPHATALRALS----T-SEHGLFTARQTLPEGGDTTGSGHR----
ActVA-Orf6 GTAVVNYAQWESEQAYRVNFGADPRSAELREALSSLPGLMGP-PKAVFMTPRGAILPS-------------
YgiN       PDSIVMIEQWESIAHLEA-HLQTPHMKAYSEAVKGDV----LEMNIRILQPGI------------------
AknX       PGQYVNVAEWRDAASFRA-AVSHPDFGPHASALRALS----E-SRPALYEARLRCESGTDRSGAER-----
TcmH       -EQVVNYAQWRSEADFRA-MHADPRLQPHFDYCRSVS----R-PKPIFCEVTHSFGATSPEGA--------
peucetius  RPQYVNIAVWDDEASFRA-AVAHPEFPAHAAALRALS----T-SEPTLYRHRQIRVAPDVPAVSGPGGRTT
steffi     QDRYINIALWEDAQSWRN-AVAHPGFQDHAKEIRART----T-NVGELYAPRQSFSVK-------------
CosX       PHSYVNIARWADVASFRA-AVGQSDFRPHAEALRAIS----T-SSSNLYLER-RSATGEAR----------
```

FIGURE 4: Structure-based amino acid sequence alignment of SnoaB with monooxygenases from the same fold family. Note that the overall sequence identity between SnoaB and Ygin is only 6% and might reflect convergent rather than divergent evolution. The residues important for catalysis by SnoaB are shown with black background, and the PGF motif is highlighted by a gray background. ActVA is from *S. coelicolor* A3(2) (GI46812), AknX is from *Streptomyces* sp. SPB74 (EDY42533.1), TcmH is from *S. glaucescens* (P39889), peucetius denotes a putative oxygenase from *S. peucetius* (AAA65205.1), steffi is a putative oxygenase from *S. steffisburgensis* (CAJ42321.1), and CosX is a putative oxygenase from *S. olindensis* (ABC00737.1). Ygin is a quinol monooxygenase from *E. coli* (CAQ33368).

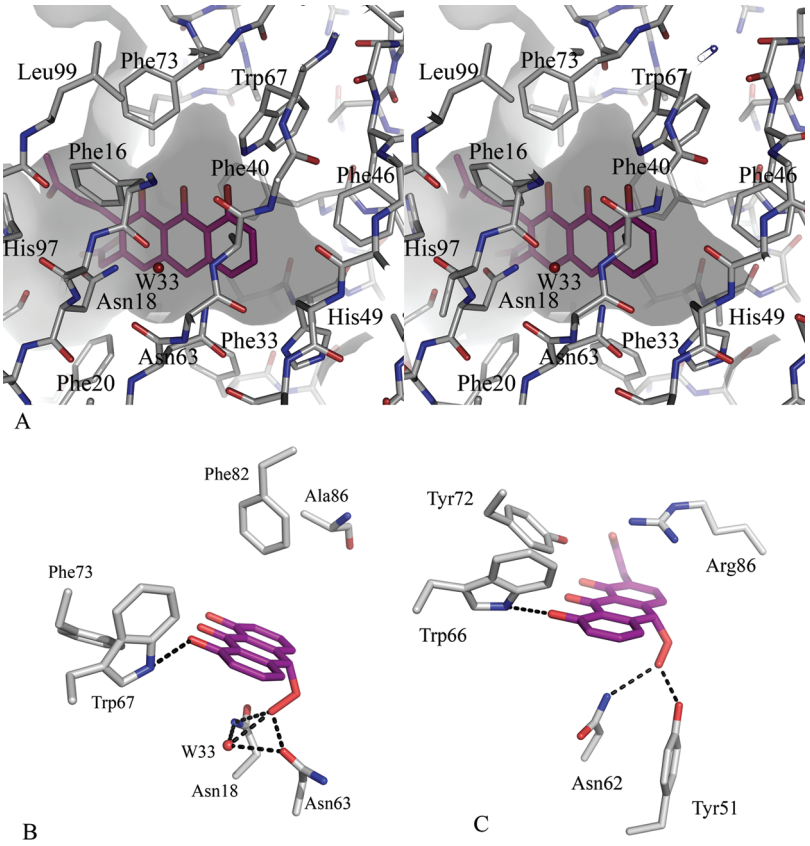

FIGURE 5: Active site and catalytic machinery in SnoaB and ActVA-Orf6. (A, top) The substrate 12-deoxynogalonic acid modeled in the active site of SnoaB. The active site cavity is indicated in gray. The shape of the cavity was calculated with the program CASTp (*52*). (B, bottom left) Model of the semiquinone peroxide intermediate of dithranol in the active site of SnoaB. (C, bottom right) Model of the semiquinone peroxide intermediate of acetyldithranol in the active site of ActVA-Orf6. Dotted lines indicate hydrogen bonds (distance between heteroatoms < 3.2 Å). The model was adapted from ref 4.

Aciadinus ambivalens (PDB id 2CB2) (*45*) and, intriguingly, the tetracenomycin F2 cyclase from *Streptomyces glaucescens* (1TUW) (*46*).

The list of the structural homologues also contains two characterized cofactor-independent monooxygenases: the quinol monooxygenase YgiN from *E. coli* (1R6Y) (*9*) and ActVA-Orf6 from actinorhodin biosynthesis from *S. coelicolor* (1N5Q) (*4*). Both enzymes convert phenolic substrates to quinone products, similarly to SnoaB, and the following comparisons will focus on these two enzymes. These homologues share, in addition to the overall ferredoxin-like fold, the mode of dimerization via strand swapping. The rmsd difference of the superposition of the main chain atoms of SnoaB and YgiN is 2.0 Å with 91 aligned residues and 1.7 Å with 88 aligned residues for the superposition with ActVA-Orf6. The amino acid sequence identity between SnoaB and ActVA-Orf6 is 16% and only 6% between SnoaB and YgiN.

Trp67 is the only active site residue conserved in the three oxygenases SnoaB, ActVA-Orf6, and Ygin (Figure 4). In addition, ActVA-Orf6 contains an asparagine residue (Asn62) at a position corresponding to Asn63 in SnoaB, and the hydrophobic active site residues Ala65 and Phe46 (as numbered in SnoaB) are conserved between the two enzymes. The overall size and shape of the active site cavities are similar, although the active site of SnoaB appears to be of even more hydrophobic character than that of ActVA-Orf6. The active site of YgiN is, as expected in light of the smaller substrate, smaller in volume. In addition to Trp67, Phe33 (Phe24 in YgiN) is the only amino acid residue conserved between the active sites of SnoaB and YgiN. The latter does not possess the PGF motif observed in homologues of *Streptomyces* origin, although the glycine residue of this motif is conserved.

Active Site and Ligand Modeling. The active site cavity is lined mainly by hydrophobic residues. The active sites of the SnoaB subunits in the two space groups are very similar, the only significant difference being the dual conformation of Asn18 in the tetragonal crystal form. In addition, there are slight variations in orientation of phenylalanine side chains in the active sites of different molecules in the orthorhombic crystals. An inspection of the active site cavity suggests four amino acids that might be potential catalytic residues: Trp67, Asn18, Asn63, and His49 (Figure 5A). A water molecule, Wat33 in subunit B and WAT147 in subunit A, is bound between residues Asn18 and Asn63. The water molecule is well-defined in electron density, and its *B*-factor (25.9 $Å^2$) is similar to those of the neighboring residues. In subunit B, it is within hydrogen-bonding distance to the two asparagines as well as to the main chain oxygen of Phe16. Residues Asn18, Asn63, and His49 form a hydrogen-bonding network via this water molecule, and the network is connected to the solvent outside the active site via Ser95, His49, and His98. In subunit A, it is shifted from its position in subunit B but is still within hydrogen-bonding distance to the side chains of the two asparagine residues. These two water molecules are only observed in the tetragonal crystal form, possibly because in this space group SnoaB contains bound ligands in the active site.

In order to obtain a ligand complex, cocrystallization and soaking experiments were undertaken with the natural product, nogalonic acid, as well as with product analogues. In addition,

the inactive mutant Asn63Ala was cocrystallized and soaked with several substrate/product analogues. However, no difference electron density which could be unambiguously assigned to these ligands was observed in the electron density maps obtained from orthorhombic crystals. The failure to obtain defined enzyme−product complexes may be due to weak affinity of the product to the active site of SnoaB and/or the limited solubility of these compounds which disfavors a high enough concentration of the ligands to saturate the active sites.

In the case of the tetragonal crystal form, cocrystallized with the reaction product danthrone, difference electron density indicating a bound ligand was observed in the active sites of both subunits. However, it was not possible to fit danthrone unambiguously into this electron density, suggesting that a different ligand was bound to the enzyme. Because the identity of the bound compound is unknown, we did not include any model of the ligand in the final cycles of refinement and the deposited atomic coordinates.

In the absence of a well-defined structure of a complex with bound substrate or product analogues, substrate binding to SnoaB was modeled manually. This was based on the observed difference electron densities in the active sites of SnoaB in the tetragonal crystal form and substrate complexes of the homologous enzyme, ActVA-Orf6 (*4*). The active site of SnoaB is predominantly hydrophobic and narrow, which restricts the potential binding modes of the large tricyclic substrate. Modeling was carried out both with dithranol, which was used in kinetic assays, and with the natural substrate, 12-deoxynogalonic acid (Figure 5A). There is not enough space in the active site pocket to accommodate the aliphatic side chains attached to ring B of 12-deoxynogalonic acid, and they were therefore modeled pointing out from the active site. The substrate was placed in the same orientation as in ActVA-Orf6, with the C-4 hydroxyl group within hydrogen-bonding distance to the nitrogen atom of the side chain of Trp67. This is the only potential hydrogen bond between dithranol and the enzyme, but the natural substrate may form an additional hydrogen bond with His97 via the oxygen at carbon 9. Carbon atom C-12 of the substrate is at a distance of 3.4 Å to Asn63, 4.1 Å to Asn18, and 4.2 Å to Wat33. In this orientation, Phe40 is positioned well to contribute to the proper alignment of the aromatic polycyclic substrate for the reaction via stacking interactions.

Also, the semiquinone peroxide intermediate of dithranol was modeled in the active site (Figure 5B). The distal oxygen of the hydroperoxide intermediate is at hydrogen-bonding distance to Asn18 and Asn63 as well as to the water molecule Wat33.

Mutational Analysis. Based on sequence conservation and structure analysis, five active site mutants were produced and analyzed: Trp67Phe, Asn63Ala, Asn18Ala, His49Ala, and Arg90Gln. The kinetic parameters of the mutants are summarized in Table 3. The mutation Trp67Phe decreased the enzyme activity to 1% of WT activity. This drop in catalytic activity is consistent with the strict conservation of this residue (Figure 4), suggesting an important contribution to rate enhancement by SnoaB. The mutations at positions Asn18Ala and Asn63Ala also seriously compromised enzymatic activity to a residual V_{max} of 1.6% and 1.1% of WT, respectively, implying important roles in the catalytic mechanism of SnoaB (Table 3).

Residue Arg86 in ActVA-Orf6 (Figure 5C) has previously been suggested as a catalytically significant residue involved in the deprotonation and, thereby, activation of the substrate (*4*). It was also suggested to be structurally conserved, corresponding to Arg90 in SnoaB. Replacement of Arg90 in SnoaB to glutamine led to a moderate drop in catalytic activity, which is not consistent with a catalytic role of this residue. This is not surprising, considering the position of the residue in the structure of the enzyme (Figure 6). A structural alignment of SnoaB with ActVA-Orf6 shows that these two arginine residues, Arg86 in ActVA-Orf6 and Arg90 in SnoaB, are structurally not equivalent but are shifted by four residues in helix 3 in the crystal structures (Figures 4 and 6). The side chain of Arg90 in SnoaB is pointing away from the active site and is too far from the substrate binding pocket to form an interaction with the substrate as observed with Arg86 in ActVA-Orf6. These observations suggest that ActVA-Orf6 shows differences in the mechanism of oxygen activation to other family members, which were indicated already by the low degree of sequence conservation.

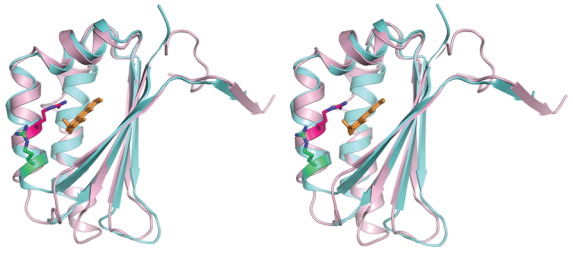

FIGURE 6: Superposition of SnoaB (turquoise) and ActVA-Orf6 (pink). The substrate bound in ActVA-Orf6, acetyldithranol, is shown in orange. The two arginine residues, Arg90 (green) in SnoaB and Arg86 (red) in ActVA-Orf6, shown as stick models, are not structurally equivalent.

His49 is located in the active site of SnoaB in the vicinity of the substrate and as such might potentially be involved in proton transfer steps and/or radical formation. However, replacement of this residue into alanine only moderately affects the catalytic activity (V_{max} 20% of wild-type enzyme) and K_M value, implying no essential catalytic or substrate binding role of this residue.

The SnoaB mutants were properly folded. All enzyme variants showed nearly identical CD spectra, characteristic for a properly folded protein with α and β secondary structure elements (data not shown). These observations imply that the reduction in enzymatic activity upon residue substitution is not due to large-scale structural disturbances. In addition, the crystal structure of the Asn63Ala mutant at 2.5 Å resolution (Table 2) showed an active site structure very similar to that of wild-type SnoaB.

DISCUSSION

Two possible catalytic mechanisms have been suggested for SnoaB-like cofactor-independent monooxygenases from polyketide biosynthesis. Shen and Hutchinson (*19*) proposed a radical mechanism for TcmH, in which the enzyme abstracts a hydrogen atom from the substrate to form a phenolic radical intermediate and an enzyme-bound radical species. An alternative mechanism was proposed for AknX by Chung et al. (*18*), who concluded that catalysis proceeds via a carbanion intermediate. On the basis of high-resolution crystal structures of ActVA-Orf6, Vallone and co-workers (*4*) also derived a substrate−carbanion-based mechanism for this enzyme. Residues Trp66, Tyr72, and Arg86 in ActVA-Orf6 were suggested to be responsible for the initial deprotonation of the substrate. In the light of the structural and biochemical data available for SnoaB these two reaction mechanisms were considered.

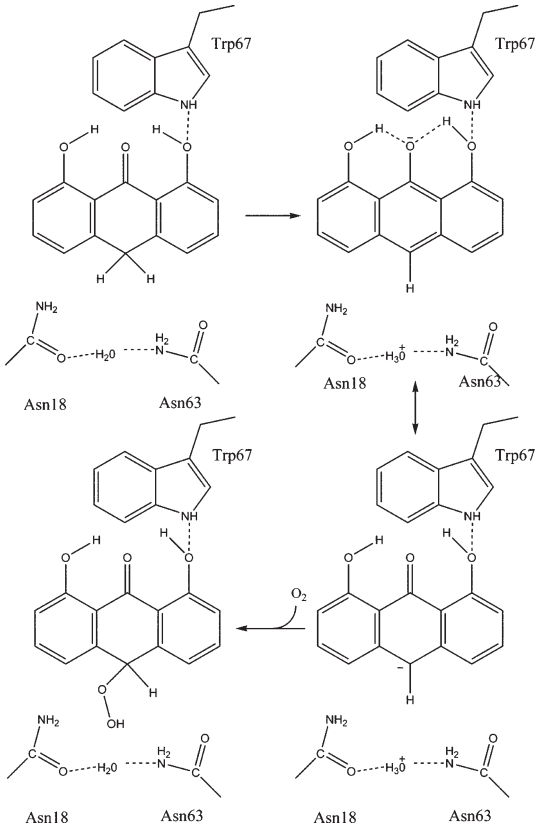

FIGURE 7: Proposed mechanism for formation of the peroxy intermediate by SnoaB.

Nonenzymatic autoxidation of anthrones occurs via a resonance-stabilized anion, which is prone by one-electron transfer to form an anthrone free radical (*47*). Mechanistically, a SnoaB-catalyzed reaction proceeding via a substrate-derived carbanion intermediate would be initiated by deprotonation of the substrate, 12-deoxynogalonic acid (Figure 7) or, alternatively, by binding preferentially the carbanionic form of the substrate. In ActVA-Orf6 (*4*), proton abstraction is proposed to occur via the keto−enol tautomer of the substrate, 6-dioxydihydrokalafungin, at the C-13 oxygen by the Trp66-Tyr72-Arg86 triad. In SnoaB the residues structurally equivalent to Tyr72 and Arg86 are replaced by phenylalanine and alanine, respectively, and there are no other potential catalytic groups that could act as a base to abstract the proton from 12-deoxynogalonic acid in the vicinity of the corresponding substrate oxygen atom. Hence, formation of the substrate carbanion, if promoted by the enzyme, must utilize a different catalytic machinery. The structure of SnoaB suggests that proton abstraction from the substrate could occur via the Asn18-Asn63-water triad close to the C-12 carbon atom of 12-deoxynogalonic acid (Figure 7). This triad is located on the opposite side of the ring system compared to the Trp66-Tyr72-Arg86 triad in ActVA-Orf6. Proton abstraction would be facilitated by the inherent acidity of the C-12 protons due to resonance stabilization of the negative charge of the resulting anion over the tricyclic aromatic ring system and could be further stabilized via a hydrogen-bonding network involving the C-4 hydroxyl group of the substrate and Trp67 (Figure 7).

The carbanion, once formed, can react with molecular oxygen via a single electron transfer step to form a caged substrate radical−superoxide radical anion pair that can recombine to a hydroperoxy anion intermediate, reminiscent of catalysis by flavin-dependent monooxygenases. The peroxide intermediate is stabilized by hydrogen bonding to asparagines 18 and 63, as well as to the putative catalytic water (Wat33) (Figure 5B). Protonation of this intermediate, possibly via the catalytic water molecule of the Asn18-Asn63-Wat33 triad, results in the final products, nogalonic acid and water. The mechanistic scenario is not only supported by the three-dimensional structure and modeling of substrate binding in the active site but is also consistent with the results from the mutagenesis studies. Substitution of Trp67 by a phenylalanine residue does not completely abolish catalytic activity, not in SnoaB or the close relative AknX (*18*). It is likely to have a role in binding the substrate and aligning it in an appropriate position in the active site. Replacements of Asn18 and Asn63 have also significant effects on catalytic activity, emphasizing the important roles of these two residues in catalysis, i.e., positioning and activation of the catalytic water molecule (Figure 5B). While the catalytic triad Asn18 and Asn63 is conserved in the closest relatives of SnoaB, it is not in ActVA-Orf6, a more distant member of this family of cofactor-independent monooxygenases (Figure 4). In this enzyme, a tyrosine residue, Tyr51, which is not structurally equivalent to Asn18 in SnoaB, has been invoked in the stabilization of the peroxy intermediate (Figure 5C).

Our findings are less supportive of the second mechanistic scenario that assumes formation of an enzyme-bound radical. Examination of the substrate binding pocket in SnoaB reveals only two potential amino acid side chains that are amenable to radical formation: His49 and Trp67. Replacement of His49 using site-directed mutagenesis resulted in an enzyme variant that displayed significant residual activity demonstrating that it is not essential for catalysis. The Trp67Phe mutant is more impaired in catalytic activity than the His49Ala variant; nevertheless, the remaining catalytic activity argues against a crucial role of this residue as the enzyme-bound radical species in a radical mechanism. These observations are in line with a study on AknX where replacement of Trp67 resulted in a mutant enzyme with significant remaining activity (V_{max} approximately 20% of wild type) (*18*). In the case of SnoaB and other related cofactor-independent oxygenases, mechanisms that suppose an enzyme-bound radical assume abstraction of a hydrogen atom from the substrate (*19*), i.e., imply formation of a reduced tryptophan radical. On chemical grounds this appears less likely. In all established enzyme mechanisms that feature a tryptophan radical intermediate it is in the oxidized state, either as a cationic or neutral species (ref *48* and references cited therein). Reduced tryptophan radicals are rare, and we could find only one report in the literature that describes a reduced tryptophan radical, generated in solution by X-ray irradiation of L-tryptophan (*49*).

In conclusion, our structural and functional data on SnoaB, a cofactor-independent monooxygenase involved in aromatic polyketide biosynthesis, support a carbanion mechanism of oxygen activation. This is in line with structural studies of ActVA-Orf6 and other monooxygenases from different fold families such as DpgC from vancomycin biosynthesis (*6*) and urate oxidase (*8*), that all support carbanion mechanisms. So far, no firm and compelling evidence has been provided that any of these enzymes performs the reaction via a radical mechanism. Rather, formation of a carbanion intermediate appears to be a common mechanistic trait in these enzymes, not related by sequence or fold (*3*). Enzyme-catalyzed reactions of carbanions with oxygen are not without precedence, and its most prominent representative is the oxygenation reaction of ribulose-1,5-bisphosphate carboxylase/oxygenase (Rubisco). In a seminal paper,

Abell and Schloss (*50*) proposed 2 decades ago that similar enzyme-catalyzed reactions of carbanions with oxygen might also be observed with other enzymes.

ACKNOWLEDGMENT

We gratefully acknowledge access to synchrotron radiation at the ESRF, Grenoble, France, and MAXlab, Lund, Sweden.

REFERENCES

1. Klinman, J. (2001) Life as aerobes: are there simple rules for activation of dioxygen by enzymes? *J. Biol. Inorg. Chem. 6*, 1–13.
2. Fetzner, S. (2007) Cofactor-independent oxygenases go it alone. *Nat. Chem. Biol. 3*, 374–375.
3. Fetzner, S. (2002) Oxygenases without requirement for cofactors of metal ions. *Appl. Microbiol. Biotechnol. 60*, 243–257.
4. Sciara, G., Kendrew, S. G., Miele, A. E., Marsh, N. G., Federici, L., Malatesta, F., Schimperna, G., Savino, C., and Vallone, B. (2003) The structure of ActVA-Orf6, a novel type of monooxygenase involved in actinorhodin biosynthesis. *EMBO J. 22*, 205–215.
5. Beinker, P., Lohkamp, B., Peltonen, T., Niemi, J., Mäntsälä, P., and Schneider, G. (2006) Crystal structures of SnoaL2 and AclR: two putative hydroxylases in the biosynthesis of aromatic polyketide antibiotics. *J. Mol. Biol. 359*, 728–740.
6. Widboom, P. F., Fielding, E. N., Liu, Y., and Bruner, S. D. (2007) Structural basis for cofactor-independent dioxygenation in vancomycin biosynthesis. *Nature 447*, 342–345.
7. Stec, B., and Stieglitz, K. A. (2008) Not so clear on oxygen. Comment on structural basis for cofactor-independent dioxygenation in vancomycin biosynthesis by Widboom et al. (2007), *Nature* (*London*) *447*, 342−345. *Acta Crystallogr. D64*, 1000–1002.
8. Colloc'h, N, Gabison, L, Monard, G, Altarsha, M, Chiadmi, M, Marassio, G, Sopkova-de Oliveira Santos, J, El Hajji, M, Castro, B, Abraini, J. H., and Prangé, T. (2008) Oxygen pressurized X-ray crystallography: probing the dioxygen binding site in cofactorless urate oxidase and implications for its catalytic mechanism. *Biophys. J. 95*, 2415–2422.
9. Adams, M. A., and Jia, Z. (2005) Structural and biochemical evidence for an enzymatic quinone redox cycle in *Escherichia coli*: identification of a novel quinol monooxygenase. *J. Biol. Chem. 280*, 8358–8363.
10. Frerichs-Deeken, U., Ranguelova, K., Kappl, R., Hüttermann, J., and Fetzner, S. (2004) Dioxygenases without requirement for cofactors and their chemical model reaction: compulsory order ternary complex mechanism of 1*H*-3-hydroxy-4-oxoquinaldine 2,4-dioxygenase involving general base catalysis by histidine 251 and single-electron oxidation of the substrate dianion. *Biochemistry 43*, 14485–14499.
11. Ylihonko, K., Tuikkanen, J., Jussila, S., Cong, L., and Mäntsälä, P. (1996) A gene cluster involved in nogalamycin biosynthesis from *Streptomyces nogalater:* sequence analysis and complementation of early-block mutations in the anthracycline pathway. *Mol. Gen. Genet. 251*, 113–120.
12. Koskiniemi, H., Grocholski, T., Schneider, G., and Niemi, J. (2009) Expression, purification and crystallization of the cofactor-independent monooxygenase SnoaB from the nogalamycin biosynthetic pathway. *Acta Crystallogr. F65*, 256–259.
13. Räty, K., Kantola, J., Hautala, A., Hakala, J., Ylihonko, K., and Mäntsälä, P. (2002) Cloning and characterization of *Streptomyces galilaeus* aclacinomycins polyketide synthase (PKS) cluster. *Gene 293*, 115–122.
14. Motamedi, H., and Hutchinson, C. R. (1987) Cloning and heterologous expression of a gene cluster for the biosynthesis of tetracenomycin C, the anthracycline antitumor antibiotic of *Streptomyces glaucescens*. *Proc. Natl. Acad. Sci. U.S.A. 84*, 4445–4449.
15. Madduri, K., and Hutchinson, C. R. (1995) Functional characterization and transcriptional analysis of a gene cluster governing early and late steps in daunorubicin biosynthesis in *Streptomyces peucetius*. *J. Bacteriol. 177*, 3879–3884.
16. Kendrew, S. G., Hopwood, D. A., and Marsh, E. N. (1997) Identification of a monooxygenase from *Streptomyces coelicolor* A3(2) involved in biosynthesis of actinorhodin: purification and characterization of the recombinant enzyme. *J. Bacteriol. 179*, 4305–4310.
17. Okamoto, S., Taguchi, T., Ochi, K., and Ichinose, K. (2009) Biosynthesis of actinorhodin and related antibiotics: discovery of alternative routes for quinone formation encoded in the *act* gene cluster. *Chem. Biol. 16*, 226–236.
18. Chung, J. Y., Fujii, I., Harada, S., Sankawa, U., and Ebizuka, Y. (2002) Expression, purification, and characterization of AknX anthrone oxygenase, which is involved in aklavinone biosynthesis in *Streptomyces galilaeus*. *J. Bacteriol. 184*, 6115–6122.
19. Shen, B., and Hutchinson, R. (1993) Tetracenomycin F1 monooxygenase: oxidation of a naphthacenone to a naphthacenequinone in the biosynthesis of tetracenomycin C in *Streptomyces glaucescens*. *Biochemistry 32*, 6656–6663.
20. Anderson, M. G., Khoo, C. L.-Y., and Rickards, R. W. (1989) Oxidation processes in the biosynthesis of the tetracenomycin and elloramycin antibiotics. *J. Antibiot. 42*, 640–642.
21. Fujii, I., Chen, Z.-G., Ebizuka, Y., and Sankawa, U. (1991) Identification of emodinanthrone oxygenase in fungus *Aspergillus terreus*. *Biochem. Int. 25*, 1043–1049.
22. Higuchi, R., Krummel, B., and Saiki, R. K. (1988) A general method of in vitro preparation and specific mutagenesis of DNA fragments: study of protein and DNA interactions. *Nucleic Acids Res. 16*, 7351–7367.
23. Gasteiger, E., Hoogland, C., Gattiker, A., Duvaud, S., Wilkins, M. R., Appel, R. D., and Bairoch A. (2005) Protein Identification and Analysis Tools on the ExPASy Server, in The Proteomics Protocols Handbook (Walker J. M., Ed.) pp 571−607, Humana Press, Totowa, NJ.
24. Cross, E. J., and Perkin, A. G. (1930) Reduction products of the hydroxyanthraquinones. Part XI. *J. Chem. Soc.,* 292–308.
25. Kantola, J., Kunnari, T., Hautala, A., Hakala, J., Yliohonko, K., and Mäntsälä, P (2000) Elucidation of anthracyclinone biosynthesis by stepwise cloning of genes for anthracyclines from three diffrent *Stroptomyces* spp. *Microbiology 146*, 155–163.
26. Jansson, A., Koskiniemi, H., Erola, A., Wang, J., Mäntsälä, P., Schneider, G., and Niemi, J. (2005) Aclacinomycin 10-hydroxylase is a novel substrate-assisted hydroxylase requiring *S*-adenosyl-L-methionine as cofactor. *J. Biol. Chem. 280*, 3636–3644.
27. Kallio, P., Liu, Z., Mäntsälä, P., Niemi, J., and Metsä-Ketelä, M. (2008) Sequential action of two flavoenzymes PgaE and PgaM in angucycline biosynthesis: chemoenzymatic synthesis of gaudimycin C. *Chem. Biol. 15*, 157–166.
28. Leslie, A. G. W. (1992) Recent changes to the MOSFLM package for processing film and image plate data, Joint CCP4 + ESF-EAMCB Newsletter on Protein Crystallography, *No. 26*, Daresbury Laboratory, Daresbury, U.K.
29. Collaborative Computational Project, Number 4 (1994) The CCP4 suite: programs for protein crystallography, Acta Crystallogr. *D50*, 760−763.
30. McCoy, A. J., Grosse-Kunstleve, R. W., Adams, P. D., Winn, M. D., Storoni, L. C., and Read, R. J. (2007) *Phaser* crystallographic software. *J. Appl. Crystallogr. 40*, 658–674.
31. Murshudov, G. N., Vagin, A. A., and Dodson, E. J. (1997) Refinement of macromolecular structures by the maximum-likelihood method. *Acta Crystallogr. D53*, 240–255.
32. Emsley, P., and Cowtan, K. (2004) Coot: model-building tools for molecular graphics. *Acta Crystallogr. D60*, 2126–2132.
33. Winn, M., Isupov, M., and Murshudov, G. N. (2001) Use of TLS parameters to model anisotropic displacements in macromolecular refinement. *Acta Crystallogr. D57*, 122–133.
34. Painter, J., and Merrit, E. A. (2006) Optimal description of a protein structure in terms of multiple groups undergoing TLS motion. *Acta Crystallogr. D62*, 439–450.
35. Brunger, A. T. (2007) Version 1.2 of the crystallography and NMR system. *Nat. Protoc. 2*, 2728–2733.
36. Laskowski, R. A., MacArthur, M. W., Moss, D. S., and Thornton, J. M. (1993) PROCHECK: a program to check the stereochemical quality of protein structures. *J. App. Crystallogr. 26*, 283–291.
37. Davis, I. W., Leaver-Fay, A., Chen, V. B., Block, J. N., Kapral, G. J., Wang, X., Murray, L. W., Arendall, W. B., III, Snoeyink, J., Richardson, J. S., and Richardson, D. C. (2007) MolProbity: all-atom contacts and structure validation for proteins and nucleic acids. *Nucleic Acids Res. 35*, W375–W383.
38. Krissinel, E., and Henrick, K. (2007) Inference of macromolecular assemblies from crystalline state. *J. Mol. Biol. 372*, 774–797.
39. Schuettelkopf, A. W., and van Aalten, D. M. F. (2004) PRODRG—a tool for high-throughput crystallography of protein-ligand complexes. *Acta Crystallogr. D60*, 1355–1363.
40. Larkin, M. A., Blackshields, G., Brown, N. P., Chenna, R., McGettigan, P. A., McWilliam, H., Valentin, F., Wallace, I. M., Wilm, A., Lopez, R., Thompson, J. D., Gibson, T. J., and Higgins, D. G. (2007) ClustalW and ClustalX version 2. *Bioinformatics 23*, 2947–2948.
41. Pei, J., and Grishin, N. V. (2007) PROMALS: towards accurate multiple sequence alignments of distantly related proteins. *Bioinformatics 23*, 802–808.

42. DeLano, W. L. (2002) The PyMOL Molecular Graphics System, DeLano Scientific, Palo Alto, CA (http://www.pymol.org).
43. Holm, L., Kääriäinen, S., Rosenstrom, P., and Schenkel, A. (2008) Searching protein structure databases with DaliLite v.3. *Bioinformatics 24*, 2780–2781.
44. Wada, T., Shirouzu, M., Terada, T., Kamewari, Y., Park, S. Y., Tame, J. R., Kuramitsu, S., and Yokoyama, S. (2004) Crystal structure of the conserved hypothetical protein TT1380 from *Thermus thermophilus* HB8. *Proteins 55*, 778–780.
45. Urich, T., Gomes, C. M., Kletzin, A., and Frazão, C. (2006) X-ray structure of a self-compartmentalizing sulfur cycle metalloenzyme. *Scienc 311*, 996–1000.
46. Thompson, T. B., Katayama, K., Watanabe, K., Hutchinson, C. R., and Rayment, I. (2004) Structural and functional analysis of tetracenomycin F2 cyclase from *Streptomyces glaucescens*. A type II polyketide cyclase. *J. Biol. Chem. 279*, 37956–37963.
47. Müller, K. (1996) Antipsoriatic anthrones: aspects of oxygen radical formation, challenges and prospects. *Gen. Pharmacol. 27*, 1325–1335.
48. Pogni, R., Baratto, M. C., Giansanti, S., Teutloff, C., Verdin, J., Valderrama, B., Lendzian, F., Lubitz, W., Vazquez,-Duhalt, R., and Basosi, R. (2005) Tryptophan-based radical in the catalytic mechanism of versatile peroxidase from *Bjerkandera adusta*. *Biochemistry 44*, 4267–4274.
49. Moan, J., and Kaalhus, Olav (1974) Ultraviolet and x-ray induced radicals in frozen polar solutions of L-tryptophan. *J. Chem. Phys. 61*, 3556–3566.
50. Abell, L. M., and Schloss, J. V. (1991) Oxygenase side reactions of acetolactate synthase and other carbanion-forming enzymes. *Biochemistry 30*, 7883–7887.
51. Sultana, A, Kallio, K, Jansson, A, Wang, J-S, Niem, J, Mäntsälä, P, and Schneider, G. (2004) Crystal structure of the polyketide cyclase SnoaL reveals a novel mechanism for enzymatic aldol condensation. *EMBO J. 23*, 1911–1921.
52. Dundas, J., Ouyang, Z., Tseng, J., Binkowski, A., Turpaz, Y., and Liang, Y. (2006) CASTp: computed atas of surface topography of proteins with structural and topographical mapping of functionally annotated residues. *Nucleic Acids Res. 34*, W116–W118.